

# Fault Models in Superconducting Quantum Circuits

Qifan Huang

State Key Laboratory of Computer Science  
Institute of Software, Chinese Academy of Science  
University of Chinese Academy of Science  
Beijing, China  
huangqf@ios.ac.cn

Boxi Li

Institute of Quantum Control  
Forschungszentrum Jülich  
Jülich D-52425, German  
b.li@fz-juelich.de

Minbo Gao

State Key Laboratory of Computer Science  
Institute of Software, Chinese Academy of Science  
University of Chinese Academy of Science  
Beijing, China  
gaomb@ios.ac.cn

Mingsheng Ying

State Key Laboratory of Computer Science  
Institute of Software, Chinese Academy of Science  
Department of Computer Science, Tsinghua University  
Beijing, China  
yingms@ios.ac.cn

**Abstract**—Fault models are indispensable for many EDA tasks, so as for design and implementation of quantum hardware. In this article, we propose a fault model for superconducting quantum systems. Our fault model reflects the real fault behavior in control signals and structure of quantum systems. Based on it, we conduct fault simulation on controlled-Z gate and quantum circuits by QuTiP. We provide fidelity benchmarks for incoherent faults and test patterns of minimal test repetitions for coherent faults. Results show that with 34 test repetitions a 10% control noise can be detected, which help to save test time and memory.

**Index Terms**—superconducting quantum computing, quantum circuits, fault model, fault simulation, QuTiP.

## I. INTRODUCTION

Quantum computing is considered as one of the most promising next-generation computing technology. Over the past few decades, significant progress has been made in implementing quantum computing by real physical systems such as quantum dots, ion traps and superconducting systems. Among them, superconducting quantum systems are widely acknowledged as one of the most promising technologies. Qubits made of superconducting devices harness the advantages of scalability and stability. In particular, two qubit gates, e.g. controlled-Z (CZ) gates, have been realized in superconducting quantum systems with the optimal fidelity known as  $99.76\% \pm 0.07\%$  [1].

Real superconducting quantum devices suffer from several serious noises, including leakage, decoherence, and control pulse noises. Therefore, proper fault models of quantum gates are indispensable in various tasks of design automation for superconducting quantum circuits, e.g. testing, simulation and verification. Indeed, several faults of superconducting quantum circuits have been considered in physical experiments, and some measures to suppress these faults have been proposed. However, there still lacks an appropriate fault model for superconducting quantum circuits that is suited to various design automation issues (e.g. fault simulation and automatic test pattern generation (ATPG)).

In this work, we introduce such a fault model, which includes both coherent faults and incoherent faults. Roughly speaking, coherent faults originate from the imperfect control signals while incoherent faults are due to the interaction with environments. To test the effectiveness of our model, we conduct fault simulation on single controlled-Z gates and certain quantum circuits, using QuTiP — a popular software for simulating quantum systems — as the main simulation tool. The simulation results show that with the undesired rotation inserted in the CZ gate, the fidelity will decrease near

exponentially with an additional fluctuation when the angle is larger than 0. With a maximum 20% noise inserted in the control, the fidelity decrease 6%. Moreover, with a 10% noise inserted in all CZ gates of a 4-qubit quantum full adder, it requires 34 repetitions to detect the fault. With a 10% noise inserted in one of the CZ gates, the fault turns out to be detected in 100 to 200 repetitions, depending on the gate number.

This article is organized as follows. Section II reviews the basics of quantum gates and circuits. In section III, we recall the basic physical model of superconducting qubits. Based on it, in Section IV, we propose our fault model of superconducting quantum circuits. In section V, the simulation tool we employed, QuTiP, is briefly introduced. The last section presents the simulation results.

## II. BASICS OF QUANTUM CIRCUITS

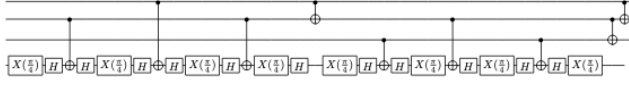
The basic data storage element in quantum circuits is quantum bit (qubit, for short). A qubit is a two-level quantum state, which can be expressed as  $|\psi\rangle = a|0\rangle + b|1\rangle$ , with the probability amplitudes satisfying  $|a|^2 + |b|^2 = 1$ . In general, a state of an  $n$ -qubit system can be represented as a superposition of the form:  $|\psi\rangle = \sum_{i=0}^{2^n-1} c_i|i\rangle$ , with integer  $i$  being identified with its binary encoding as an  $n$  bit string. An important characteristic of multi-qubit systems is the entanglement between different qubits. This means that one cannot determine the state of each qubit independently even if the qubits are distant from each other. A famous example of entanglement is the EPR pair, or 2-D Bell state,  $\frac{|00\rangle + |11\rangle}{\sqrt{2}}$ , which is the maximally entangled state of two qubits.

Quantum circuit is a basic quantum computing model consisting of quantum gates. A gate operating on an  $n$ -qubit system is mathematically modelled by a  $2^n \times 2^n$  unitary matrix, which keeps the norm of state vectors unchanged. Quantum controlled-Z (CZ) gate is one of the most commonly used two-qubit gates in superconducting quantum hardware, from which the controlled-NOT (CNOT) gate can be generated (see Fig. 1a for the unitary matrices of CZ and CNOT). In our work, we employ the quantum full adder [2] and a random circuit as examples in our fault simulation task. They consist of only single qubit gates and CNOT gates. Fig. 1b illustrates the circuit of a 4-qubit quantum full adder.

In general, to include the interaction of qubits with the environment, a noisy quantum gate needs to be described by a quantum channel instead of a unitary operation. Mathematically, the discrete-time description of a quantum channel is a superoperator transforming

$$CZ = \begin{pmatrix} 1 & 0 & 0 & 0 \\ 0 & 1 & 0 & 0 \\ 0 & 0 & 1 & 0 \\ 0 & 0 & 0 & -1 \end{pmatrix} \quad CNOT = H_2 \otimes CZ \otimes H_2 = \begin{pmatrix} 1 & 0 & 0 & 0 \\ 0 & 1 & 0 & 0 \\ 0 & 0 & 0 & 1 \\ 0 & 0 & 1 & 0 \end{pmatrix}$$

(a)



(b)

Fig. 1: (a) Matrix representation of CZ and CNOT gates. (b) The quantum circuit for four-qubit quantum full adder.

a mixed quantum state as a density matrix  $\rho$  to  $\mathcal{E}(\rho) = \sum_{i=1}^n E_i \rho E_i^\dagger$ , the set of matrices  $\{E_i\}$  is called Kraus operators. The continuous description of a quantum operation is given as the Liouville-von Neumann-Lindblad master equation [3]:

$$\frac{d\rho}{dt} = -\frac{i}{\hbar}[H, \rho] + \sum_{i=1}^{N^2-1} \gamma_i [L_i \rho L_i^\dagger - \frac{1}{2} \rho, L_i^\dagger L_i] \quad (1)$$

In the master equation, the interaction with environment is described by the collapse operator  $L_i$  together with the parameter  $\gamma_i$ .

### III. PHYSICAL MODEL OF COUPLED SUPERCONDUCTING QUBITS

Superconducting qubits encode the lowest two energy levels of the nonlinear LC circuits as  $|0\rangle$  and  $|1\rangle$ . Because of the nonlinearity brought by the Josephson junction, computational and non-computational states are separated. The most widely used design is Transmon [4], a modified charge qubit. To read out the qubit state, a cavity resonator is often coupled to the qubit before connecting it to the bus.

Since most of the techniques used in realizing the two qubit controlled-phase (CZ) gate use the avoided level-crossing between  $|11\rangle$  and  $|20\rangle$ , the second excited state  $|2\rangle$  should be taken into consideration. The standard circuit quantum electrodynamics (cQED) set-up is two superconducting qubits coupled to a common bus resonator [5]:

$$H_{\text{sys}} = \sum_{j=1,2} \omega_j (b_j^\dagger b_j) + \frac{\alpha}{2} (b_1^\dagger b_1)(b_2^\dagger b_2 - \mathbb{1}) + \omega_r c^\dagger c + \sum_{j=1,2} g_j (b_j^\dagger c + b_j c^\dagger) \quad (2)$$

where  $b_j$  and  $c$  are the destroy operators of qubit  $j$  and the resonator respectively,  $\omega_j$  is the frequency of  $j^{\text{th}}$  qubit and  $\alpha$  is the anharmonicity, which is set to be consistent for all qubits. However, in the dispersive regime, the detuning between the bus resonator and the connected qubit,  $\omega_r - \omega_j$ , is much larger than that between a pair of qubits. Therefore, the Hamiltonian of two coupled superconducting qubits can be simplified as [6]:

$$H_{\text{sys}} = \sum_j \hbar \omega_j |1\rangle\langle 1| + \hbar(2\omega_j + \alpha) |2\rangle\langle 2| + \hbar g (J_1^\dagger J_2 + J_1 J_2^\dagger) \quad (3)$$

where  $J_{1(2)}$  is the annihilation operator for a qubit system, i.e.  $J_{1(2)} = |0\rangle\langle 1| + \sqrt{2}|1\rangle\langle 2|$ . Here, the rotating wave approximation (RWA) is employed to eliminate the fast rotating terms. We denote the eigenstates of  $H_{\text{sys}}$  and the corresponding energies as  $\{|\bar{i}\bar{j}\rangle, E_{i\bar{j}}\}$ .

### IV. FAULT MODELS OF SUPERCONDUCTING QUANTUM CIRCUITS

In this section, we present our fault models for superconducting quantum circuits, which can serve as a basis for various EDA tasks for quantum computing like fault simulation and ATPG.

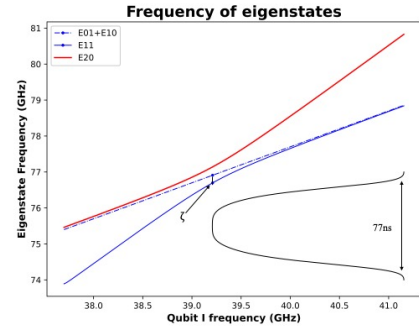


Fig. 2: Energies of eigenstates  $E_{10} + E_{01}, E_{11}, E_{20}$ . The avoided level-crossing between  $|11\rangle$  and  $|20\rangle$  and the static ZZ coupling strength  $\zeta$  is shown in the figure. The pulse with gate duration 77ns lies in the lower right corner.

We focus on the faults in the controlled-Z (CZ) gate since two qubit gates usually have lower gate fidelities than single qubit gates in real superconducting quantum hardware. In the past decades, three approaches to realizing the CZ gate have been developed: (i) cross resonance for fixed frequency qubits [7] [8] [9], (ii) adiabatic [6] [10] [11] [12] or diabatic [13] frequency tuning for frequency tunable qubits, and (iii) frequency modulation of tunable coupler [14] [15] [16]. We will mainly consider the frequency tuning approach.

#### A. Frequency Modulating Approach

Adiabatic frequency tuning approach modulates the frequency of the control qubit to harness the avoided level-crossing effect between  $|11\rangle$  and  $|20\rangle$  to activate the strong  $\sigma_z \otimes \sigma_z$  interaction. Fig. 2 shows the energy shift and a typical frequency tuning trajectory — Slepian. The unitary propagator induced by the frequency modulating is:

$$U = \begin{pmatrix} 1 & 0 & 0 & 0 \\ 0 & e^{-i\phi_{01}} & 0 & 0 \\ 0 & 0 & e^{-i\phi_{10}} & 0 \\ 0 & 0 & 0 & e^{-i\phi_{11}} \end{pmatrix} \quad (4)$$

where the relative phases  $\phi_{ij} \approx \int_0^{\text{gate}} E_{ij}(t) dt$  and  $E_{ij}(t)$  is the energy of the eigenstates  $|\bar{i}\bar{j}\rangle$  from the dynamical Hamiltonian  $H_{\text{sys}}(t)$ . Because of the avoided level-crossing, the state  $|11\rangle$  will accumulate an additional phase  $\varphi$ , that is,  $\phi_{11} = \phi_{01} + \phi_{10} + \varphi$ . Therefore, performing a CZ gate is to set  $\varphi \approx (2n+1)\pi$  where  $n$  is an integer. We mainly apply the quasi-adiabatic approach from [12] and inverse-Gaussian waveform from [11], in which the frequency changes rapidly when far from detuning and evolves adiabatically near resonance.

#### B. Fault models

Faults in superconducting quantum circuits can be divided into two categories: coherent faults and incoherent faults. In the frequency modulating approach, we consider two kinds of coherent faults and two kinds of incoherent faults:

**Coherent faults:** Coherent faults can be described by unitary fault matrices, and can be corrected according to simulation results provided by fault models. Our fault models mainly deal with the following coherent faults:

- **Pulse faults:** Pulse faults mainly arise from the errors in control parameters and gate duration. In the framework of frequency control, the additional dynamical phase is accumulated by  $\varphi(t) = \int_0^{\text{gate}} (E'_{11}(t) - E_{11}(t)) dt$ . Considering the subspace

spanned by  $\{|11\rangle, |02\rangle\}$ , the dynamical phase is expressed as [6]:

$$\varphi(t) = \int_0^{t_{\text{gate}}} \sqrt{2}g \left( \tan\left(\frac{\sqrt{2}g}{\omega_1(t) - \omega_2 + \alpha}\right) \right) dt \quad (5)$$

In this work, we apply one of the nearly optimal frequency waveforms – Slepian function [12] as the differential of the waveform to minimize the power spectral density. Because the Slepian function has no analytical form, we use its Fourier approximation:

$$\frac{d\theta}{dt} = \text{sgn}\left(t - \frac{t_{\text{gate}}}{2}\right) \sum_{n=1,2,\dots,m} \lambda_n [1 - \cos(2\pi n t / t_{\text{gate}})] \quad (6)$$

where  $\theta = \frac{\sqrt{2}g}{\omega_1(t) - \omega_2 + \alpha}$ ,  $m$  is preset and the parameters  $\{\lambda_n\}$  are determined by interpolation.

The faults come from the errors in both waveform parameters and gate duration. We mainly consider ratio and bias error for waveform parameters, and truncation error for gate duration. Therefore, suppose we use  $m$  Fourier terms to approximate Slepian function and there are  $n$  CZ gates in the quantum circuit, the number of pulse faults will be  $(2m + 1)n$ .

- **Missing gate faults:** The missing gate fault describes the error when a gate is not executed. Here we use a more realistic model. Instead of a trivial identity operation, a unitary generated by the Hamilton with no control pulse is used to include the intrinsic error of the system. Even if the control pulse is missing, there is still a remaining ZZ coupling between the two qubits, therefore the missing gate fault is also called idling fault. Consequently, this static ZZ interaction becomes the dominating term of system dynamics.

Therefore, the faulty gate — an undesired rotation induced by the missing gate fault — should be:

$$U_F \approx \text{diag}(1, 1, 1, e^{i\zeta t}) \quad (7)$$

where  $\zeta$  represents the static ZZ shift strength introduced by the coupling term. The static ZZ shift strength can be either expressed as  $\zeta = \omega_{11} - \omega_{10} - \omega_{01}$  or be measured using a Ramsey-type experiment [17]. Moreover, the period of idling is  $T = \frac{2\pi}{\zeta}$ . Consequently, the missing gate fault co So in a quantum circuit with  $n$  CZ gates after decomposing, there are totally  $n$  possible missing gate faults.

#### Incoherent faults:

- **State leakage faults:** Although the generalized leakage faults may be suppressed by improving pulse schemes, for simplicity, we assume here that, except for the  $|11\rangle - |20\rangle$  transition, the leakage population is lost and never returns back to the computational states. Under such an assumption, leakage fault will act as an incoherent fault, causing the fidelity to decrease. The overall state leakage effects can be described by a noise generator of the CZ gate [18].

$$S' = \begin{bmatrix} 0 & 0 & 0 & 0 & 0 & 0 \\ 0 & \zeta_1 & 0 & i\chi_1 e^{i\phi_1} & 0 & 0 \\ 0 & 0 & 0 & 0 & i\chi_2 e^{i\phi_2} & 0 \\ 0 & -i\chi_1 e^{-i\phi_1} & 0 & \zeta_2 & 0 & 0 \\ 0 & 0 & -i\chi_2 e^{-i\phi_2} & 0 & \zeta_3 & i\chi_3 e^{i\phi_3} \\ 0 & 0 & 0 & 0 & -i\chi_3 e^{-i\phi_3} & \zeta_4 \end{bmatrix} \quad (8)$$

The rows and columns of  $S'$  is  $|00\rangle, |01\rangle, |02\rangle, |10\rangle, |11\rangle, |20\rangle$ . Then the noisy operator of CZ gate can be expressed by  $U' =$

$U e^{iS'}$ . The decrease of fidelity due to state leakage should be  $\Delta F = 1/d^2 \text{tr}|e^{iS'}|^2$ , where  $d$  is the dimension of  $S'$ . In real physical devices the parameters are set to  $\chi_i \approx 10^{-2}, \zeta_i \approx 10^{-2}$ .

- **Decoherence:** As for superconducting quantum hardware, relatively short coherent time is a critical drawback, which means the entanglement of qubits is gradually lost due to the coupling with the environment. To describe the effect of decoherence, we use the Liouville-von Neumann-Lindblad master equation (1). For a 3-level qutrit system, the Lindblad operators for decoherence is  $L_1 = |0\rangle\langle 1| + \sqrt{2}|1\rangle\langle 2|$ ,  $L_2 = |1\rangle\langle 1| + 2|2\rangle\langle 2|$ , which represents the amplitude damping and pure dephasing effects, respectively. There are mainly two kinds of decoherence effects:

- *Amplitude damping (energy relaxation):* When amplitude damping occurs, the population of excited states will decrease, which means the  $|1\rangle$  component of the quantum state will slowly evolve to  $|0\rangle$ . Therefore, amplitude damping also indicates the energy relaxation of the system. To estimate the charge qubit's (or Transmon's) characteristic time of energy relaxation  $T_1$ , Purcell effect induced by the dispersive cavity resonator needs to be considered [4]. The altered relaxation rate induced by Purcell effect can be described as:

$$\Gamma_k^{i,i+1} = \kappa \frac{g_{i,i+1}^2}{(\omega_{i,i+1} - \omega_r)^2} \quad (9)$$

In real experiments we often take the lifetime of the resonator as  $1/\kappa = 160ns$ , while the coupling strength and anharmonicity between resonator and qubit frequency are given by the parameters of devices.

- *Phase damping (dephasing):* When phase damping occurs, the projection of the state vector onto the X-Y plane of a Bloch sphere will slowly evolve to zero, indicating that the phase information of the state vector is gradually dropped out. If there only exists the phase damping effect, then only those off-diagonal elements of the density operator will decay at the rate  $T_\phi$  without affecting diagonal elements.

Same as the relaxation rate  $\Gamma_1 = 1/T_1$ , the pure dephasing time  $T_\phi$  also comes from various physical effects. For Transmon-based qubits, the dominating effect for  $T_\phi$  is the critical current noise [4] rather than the charge noise in traditional cooper pair box (CPB) devices. Since the special design of Transmon makes charge noise decrease exponentially with the ratio of  $E_J/E_C$ , Transmon based qubits are insensitive to charge noise. In real cases, a Transmon device with  $A = 10^{-6}I_c$  and  $E_J = 35$  GHz,  $E_C = 0.4$  GHz will have the pure dephasing time  $T_\phi \approx 52\mu s$ .

The total dephasing time  $T_2$  is expressed as  $\frac{1}{T_2} = \frac{1}{2T_1} + \frac{1}{T_\phi}$ . In real superconducting quantum hardware,  $T_2$  is usually 20 – 50 $\mu s$ . [17] [4].

#### C. A general workflow for using fault models

We propose a workflow for using these fault models defined above and summarized in Table I. When conducting EDA tasks in superconducting quantum circuits, the benchmark results including only decoherence is first provided by a master equation solver. Then faults induced by leakage are considered, also as a benchmark for real quantum hardware. After that we insert noises in control coefficients and conduct fault simulation on quantum circuits and find the minimal

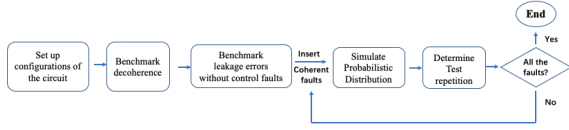


Fig. 3: A general workflow when simulating effects of fault models in superconducting quantum circuits.

test repetitions for each fault and fault coverage for a given test pattern. This workflow is visualized in Fig. 3.

## V. SIMULATION TOOL – QUTIP

Now we turn to the fault simulation of superconducting quantum circuits based on the fault models developed in the last section. We choose to use QuTiP [19] – an open-source toolbox for quantum computing in Python – to carry out our simulation tasks. QuTiP provides efficient solvers for time-dependent noisy Hamiltonians such as *mesolve* for Lindblad master equations, which represent quantum systems coupled with external environment. QuTiP also helps convert the gate-level simulation in real quantum hardware to pulse-level simulation tasks [20].

## VI. EXPERIMENTS

### A. Evaluation metrics and Simulation design

We choose the fidelity of two density operators as our metric for noisy quantum circuits. The fidelity is defined as [21]:

$$\mathcal{F}(\rho, \sigma) = \text{tr}(\sqrt{\sqrt{\rho}\sigma\sqrt{\rho}})^2 \quad (10)$$

A counterpart of density operator fidelity can also be defined for noisy quantum gates [21]:

$$\mathcal{F}(U_{\text{ideal}}, U_{\text{real}}) = \frac{1}{d^2} |\text{tr}(U_{\text{ideal}}^\dagger U_{\text{real}})|^2 \quad (11)$$

where  $d$  is the dimension of the Hilbert space on which these gates act. Both of them will be used to evaluate the effect of noise on quantum gates or circuits.

We first calibrate the pulse of the CZ gate for the maximal fidelity without decoherence and then investigate the effect of coherent faults. After that we insert coherent faults into CZ gates and carry out fault simulation on two 4-qubit quantum circuits to obtain the test repetitions. The maximum fidelity benchmark of different pulse shapes is shown in Table II, in which the pulse shape named after 'Hanning window', 'Fourier-2', 'Fourier-4' are Fourier approximations of Slepian function by using one, two and four Fourier terms each.

### B. Simulation in Single gate

1) *Missing gate faults*: We first consider fault simulation of missing gate faults. By transforming the idling Hamiltonian into the rotating frame, it can be seen that the variation of fidelity can be described by a rapid controlled-Z rotation in the two-qubit system. The missing gate fidelity at the maximum gate duration 77.0ns is 0.802. Simulation results of missing gate faults in single CZ gate show that whichever the CZ gate, simulating the circuit once suffices to detect the missing gate fault with 99% confidence level.

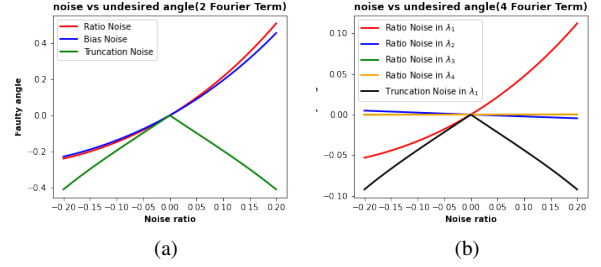


Fig. 4: (a) Undesired rotation angle brought by ratio, bias and truncation noise in  $\lambda_1$  of 'Fourier-2' waveform. (b) Undesired rotation angle brought by ratio noise in each of the coefficient of 'Fourier-4' waveform and truncation noise in  $\lambda_1$ . Both figures illustrate the theoretical estimation without numerical simulation.

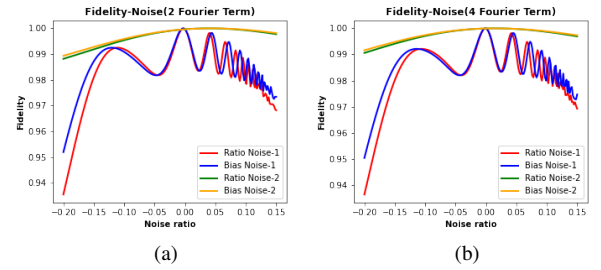


Fig. 5: (a) Fidelity versus noise in the Fourier waveform with 2 terms. (b) Fidelity versus noise in the Fourier waveform with 4 terms. Both figures illustrate the real result simulated by master equation.

2) *Control pulse error*: To test the fault effect of noises in the control coefficients, we employ the Fourier approximation of the Slepian function, shown in Eq.(12) and add ratio, bias and truncation noises to the coefficients  $\lambda_n$ .

$$\frac{d\theta}{dt} = \text{sgn}(t - \frac{t_{\text{gate}}}{2}) \sum_{n=1}^m \lambda_n [1 - \cos(2\pi n t / t_{\text{gate}})] \quad (12)$$

We use the gate duration at the optimal gate fidelity point and then insert ratio, bias and truncation faults into the parameters. We then compute the theoretical undesired rotation angle and the fidelity of the noisy gate. Fig. 4 illustrates the undesired rotation angle versus the noise ratio. It indicates that truncation noise brings a linear undesired angle to the gate while the angle brought by ratio and bias noise is approximately quadratic. Moreover, since  $\lambda_1$  is the dominating coefficient in the pulse, the noise in  $\lambda_n, n > 1$  could be ignored while the noise in  $\lambda_1$  is present.

Fig. 5 shows the fidelity versus the noise ratio obtained by real results simulated by master equation. Slightly different from the theoretical results illustrated in Fig. 4, The experimental fidelity goes through more oscillations, which are very common indications for off-resonant leakage-like dynamics.

3) *Decoherence*: In this part we evaluate the effect of decoherence. We set the energy relaxation time  $T_1 = 100\mu s$  and total dephasing time  $T_2^* = 20\mu s$ . We employ a two-qubit random circuit with  $m$  layers to benchmark the decoherence effect. In each layer there are two single qubit gates randomly selected from the set  $\{R_x(\pi/4), R_y(\pi/4), R_z(\pi/4)\}$  together with a CNOT gate with a random control qubit. We evaluate the gate fidelity with decoherence

| Faults              | Category   | Physical Factors            | Fault effect                               |
|---------------------|------------|-----------------------------|--|
| Pulse faults        | Coherent   | Noise in control parameters | Undesired ZZ rotation                      |
| Leakage faults      | Incoherent | Non-adiabaticity in pulse   | Population decrease of computational basis |
| Decoherence         | Incoherent | Superconducting system      | off-diagonal element dissipation           |
| Missing gate faults | Coherent   | Static ZZ shift             | Undesired ZZ rotation                      |

TABLE I: A brief summary to fault models in superconducting quantum circuits.

TABLE II: Simulation results of simple control pulses. The accuracy of the gate time is limited to 0.1ns.

| Pulse shape | Max Fidelity | Pulse shape    | Max Fidelity |
|-------------|--------------|----------------|--------------|
| Square      | 99.30%       | Hanning window | 99.93%       |
| Cosine      | 99.90%       | Fourier-2      | 99.95%       |
| Slepian     | 99.99%       | Fourier-4      | 99.98%       |

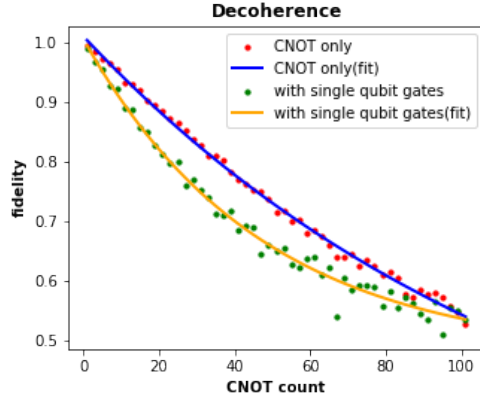


Fig. 6: Fidelity change brought by decoherence. The experimental data are shown together with the fitted curves.

in this circuit with depth ranging from 1 to 101, and try to fit exponential curves using the experimental data. The experimental and fitting results are shown in Fig. 6.

### C. Simulation in multi-qubit circuits

In this section we conduct fault simulation in multi-qubit circuits and consider the minimal test repetitions for a given fault. For each test pattern we generate a fault-free output distribution and a faulty one. Then we generate observations by randomly sampling from the faulty output distribution and perform multivariate hypothesis testing by using chi-square values. Under null hypothesis, the chi-square value between the faulty and fault-free output should follow the chi-square distribution:

$$\sum_{j=1}^J \frac{(n_j - \mu_j)^2}{\mu_j} \sim \chi_{J-1}^2 \quad (13)$$

We set the critical value as 0.99. Since the chi-square test is carried out by random sampling, for each test pattern we repeat the experiment for 50 times and use the average number of samples as the test repetition.

We conduct our experiments on a 4-qubit quantum full adder and a 4-qubit random circuit with the aid of the method in [22]. The random circuit is shown in Fig. 7. Our experiments mainly include two parts:

- 1) We add control errors in all of the CZ gates in each of the two circuits and obtain the minimal test repetition and

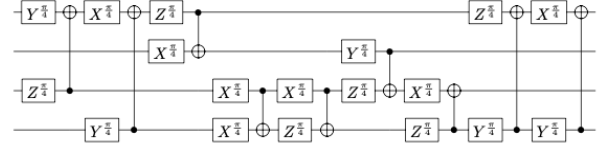
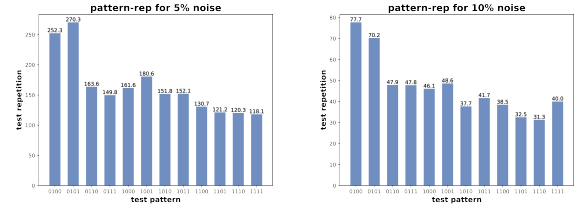
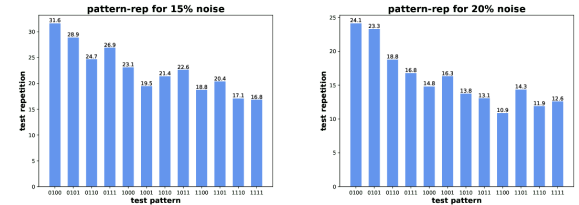


Fig. 7: The 4-qubit random circuit with 9 CZ gates for fault simulation.



(a) Test repetition for 5% noise (b) Test repetition for 10% noise



(c) Test repetition for 15% noise (d) Test repetition for 20% noise

Fig. 8: Test repetitions for different levels of errors inserted in all of the CZ gates of 4-qubit quantum full adder. The results are averaged over 50 times of sampling.

the corresponding test pattern for different levels of errors. The results of this part are shown in Fig. 8 and Fig. 9. We find that the minimal test repetition decreases exponentially, which corresponds to the variation of fidelity. Moreover, the test repetitions of random circuit when error is small are prominently larger than those of full adder, which may be explained by the more evenly output distribution of the random circuit. At last, the results show that the best test pattern, i.e., the one with the lowest number of repetition, depends both on the types of the circuit and the strength of the errors. However, for the same circuit, a sufficiently good candidate may exist, e.g., 0111 for the random circuit.

- 2) We separately add control noises on different CZ gates in the 4-qubit quantum full adder, one at a time, and find the minimal test repetition for each fault model with certain scales of noises. The results of this part are shown in Fig. 10. Results shows that the faults in number 1,3,5,7 is harder to detect than other CZ gates.

## VII. CONCLUSION

In this work we present a fault model for noisy superconducting quantum circuits, including control pulse faults, state leakage faults, decoherence faults and missing gate faults. There are totally  $(2m+2)n$  faults that need to be considered in control signals, where  $n$  is the number of CZ gates and  $m$  is the Fourier terms used in approximation. Using this model, we conducted fault simulation on single controlled-Z gate and on certain quantum circuits consisted of single qubit gates and CNOT gates. Simulation results of the noises show that the fidelity decreases exponentially with the noise, and a 10% error in all CZ gates in a 4-qubit full adder takes 34 test repetitions to detect. Moreover, the noise inserted in one of the CZ gates will lead to either undetectable faults or faults that are detectable within 100 to 200 test repetitions. We expect that this work lay a foundation for some future quantum EDA works.

## REFERENCES

- [1] Y. Sung *et al.*, "Realization of high-fidelity cz and ZZ-free iswap gates with a tunable coupler," *Phys. Rev. X*, vol. 11, p. 021058, 2 Jun. 2021. DOI: 10.1103/PhysRevX.11.021058. [Online]. Available: <https://link.aps.org/doi/10.1103/PhysRevX.11.021058>.
- [2] C.-Y. Hsieh, C.-H. Wu, C.-H. Huang, H.-S. Goan, and J. C. Mo Li, "Realistic fault models and fault simulation for quantum dot quantum circuits," in *2020 57th ACM/IEEE Design Automation Conference (DAC)*, 2020, pp. 1–6. DOI: 10.1109/DAC18072.2020.9218573.
- [3] H. P. Breuer and F. Petruccione, *The Theory of Open Quantum Systems*. The Theory of Open Quantum Systems, 2006.
- [4] J. Koch *et al.*, "Charge-insensitive qubit design derived from the cooper pair box," *Physical Review A*, vol. 76, no. 4, Oct. 2007, ISSN: 1094-1622. DOI: 10.1103/physreva.76.042319.
- [5] E. Magesan and J. M. Gambetta, "Effective hamiltonian models of the cross-resonance gate," *Physical Review A*, vol. 101, no. 5, May 2020. DOI: 10.1103/physreva.101.052308.
- [6] T. Wang *et al.*, "Experimental realization of a fast controlled-z gate via a shortcut to adiabaticity," *Phys. Rev. Applied*, vol. 11, p. 034030, 3 Mar. 2019. DOI: 10.1103/PhysRevApplied.11.034030.
- [7] C. Rigetti and M. Devoret, "Fully microwave-tunable universal gates in superconducting qubits with linear couplings and fixed transition frequencies," *Phys. Rev. B*, vol. 81, p. 134507, 13 Apr. 2010. DOI: 10.1103/PhysRevB.81.134507.
- [8] J. L. Allen, R. L. Kosut, J. Joo, P. J. Leek, and E. Ginossar, "Optimal control of two qubits via a single cavity drive in circuit quantum electrodynamics," *Physical Review A*, vol. 95, p. 042325, 2017.
- [9] V. Tripathi, M. Khezri, and A. N. Korotkov, "Operation and intrinsic error budget of a two-qubit cross-resonance gate," *Physical Review A*, vol. 100, no. 1, Jul. 2019. DOI: 10.1103/physreva.100.012301.
- [10] L. DiCarlo *et al.*, "Demonstration of two-qubit algorithms with a superconducting quantum processor," *Nature*, vol. 460, no. 7252, pp. 240–244, Jun. 2009, ISSN: 1476-4687. DOI: 10.1038/nature08121.
- [11] J. Ghosh, A. Galiutdinov, Z. Zhou, A. N. Korotkov, J. M. Martinis, and M. R. Geller, "High-fidelity controlled- $\sigma^Z$  gate for resonator-based superconducting quantum computers," *Phys. Rev. A*, vol. 87, p. 022309, 2 Feb. 2013. DOI: 10.1103/PhysRevA.87.022309.
- [12] J. M. Martinis and M. R. Geller, "Fast adiabatic qubit gates using only  $\sigma_z$  control," *Physical Review A*, vol. 90, no. 2, Aug. 2014, ISSN: 1094-1622. DOI: 10.1103/physreva.90.022307.
- [13] R. Barends *et al.*, "Diabatic gates for frequency-tunable superconducting qubits," *Physical review letters*, vol. 123, no. 21, p. 210501, 2019.

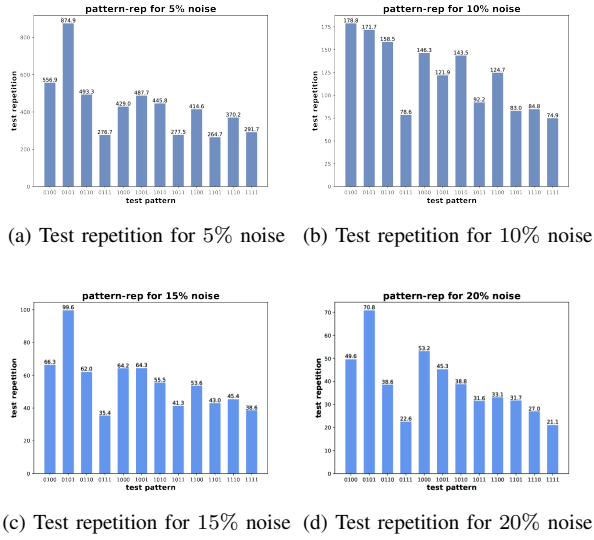


Fig. 9: Test repetitions for different levels of errors inserted in all of the CZ gates of 4-qubit random circuit. The results are averaged over 50 times of sampling.

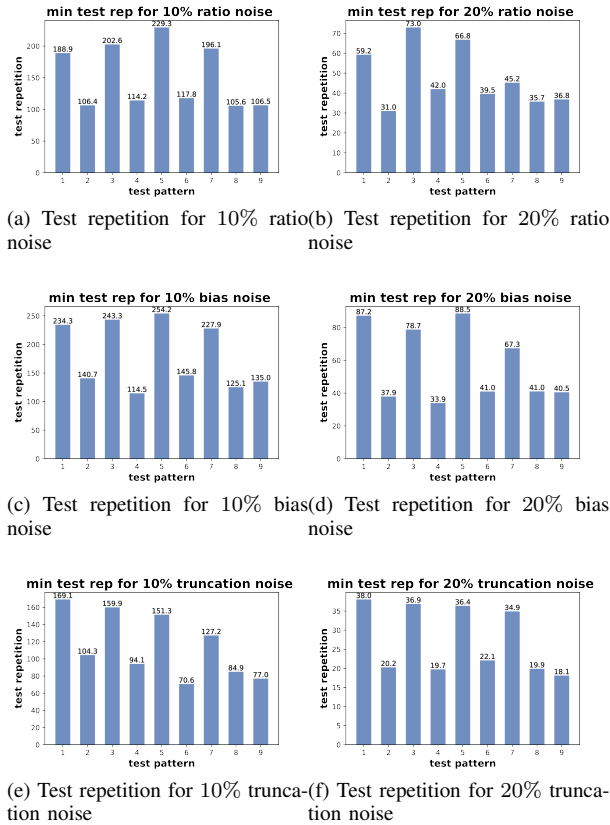


Fig. 10: Minimal test repetitions for a quantum full adder with errors inserted in one of the CZ gates.

- [14] N. Didier, E. A. Sete, M. P. da Silva, and C. Rigetti, “Analytical modeling of parametrically modulated transmon qubits,” *Phys. Rev. A*, vol. 97, p. 022330, 2 Feb. 2018. DOI: 10.1103/PhysRevA.97.022330.
- [15] J. D. Strand *et al.*, “First-order sideband transitions with flux-driven asymmetric transmon qubits,” *Phys. Rev. B*, vol. 87, p. 220505, 22 Jun. 2013. DOI: 10.1103/PhysRevB.87.220505.
- [16] S. A. Caldwell *et al.*, “Parametrically activated entangling gates using transmon qubits,” *Phys. Rev. Applied*, vol. 10, p. 034050, 3 Sep. 2018. DOI: 10.1103/PhysRevApplied.10.034050.
- [17] M. Ganzhorn *et al.*, “Benchmarking the noise sensitivity of different parametric two-qubit gates in a single superconducting quantum computing platform,” *Phys. Rev. Research*, vol. 2, p. 033447, 3 Sep. 2020. DOI: 10.1103/PhysRevResearch.2.033447.
- [18] J. Ghosh, A. G. Fowler, J. M. Martinis, and M. R. Geller, “Understanding the effects of leakage in superconducting quantum-error-detection circuits,” *Physical Review A*, vol. 88, no. 6, Dec. 2013, ISSN: 1094-1622. DOI: 10.1103/physreva.88.062329.
- [19] J. Johansson, P. Nation, and F. Nori, “Qutip 2: A python framework for the dynamics of open quantum systems,” *Computer Physics Communications*, vol. 184, no. 4, pp. 1234–1240, 2013, ISSN: 0010-4655. DOI: <https://doi.org/10.1016/j.cpc.2012.11.019>.
- [20] B. Li *et al.*, “Pulse-level noisy quantum circuits with QuTiP,” *Quantum*, vol. 6, p. 630, Jan. 2022. DOI: 10.22331/q-2022-01-24-630.
- [21] M. Raginsky, “A fidelity measure for quantum channels,” *Physics Letters A*, vol. 290, no. 1-2, pp. 11–18, Nov. 2001, ISSN: 0375-9601. DOI: 10.1016/s0375-9601(01)00640-5.
- [22] “Fault simulation for superconducting quantum circuits,” unpublished.